



1 **Temporal characteristics of atmospheric ammonia and nitrogen dioxide over China based on**
2 **emission data, satellite observations and atmospheric transport modeling since 1980**

3 Lei Liu ^a, Xiuying Zhang ^{a,*}, Wen Xu ^b, Xuejun Liu ^b, Yi Li ^c, Xuehe Lu ^a, Yuehan Zhang ^d, Wuting
4 Zhang ^{a,c}

5 ^aJiangsu Provincial Key Laboratory of Geographic Information Science and Technology, International
6 Institute for Earth System Science, Nanjing University, Nanjing 210023, China

7 ^b College of Resources and Environmental Sciences, Centre for Resources, Environment and Food
8 Security, Key Lab of Plant-Soil Interactions of MOE, China Agricultural University, Beijing 100193,
9 China

10 ^c Air Quality Division, Arizona Department of Environmental Quality, Phoenix, AZ, 85007, USA

11 ^d School of Atmospheric Sciences, Nanjing University, Nanjing, China

12 ^eJiangsu Center for Collaborative Innovation in Geographical Information Resource Development and
13 Application, Nanjing 210023, China

14 * Corresponding authors: Xiuying Zhang (lzhxy77@163.com)

15 **Abstract**

16 China is experiencing intense air pollution caused in large part by anthropogenic emissions of reactive
17 nitrogen (Nr). Atmospheric ammonia (NH₃) and nitrogen dioxide (NO₂) are the most important
18 precursors for Nr compounds (including N₂O₅, HNO₃, HONO and particulate NO₃⁻ and NH₄⁺) in the
19 atmosphere. Understanding the changes of NH₃ and NO₂ has important implications for the regulation
20 of anthropogenic Nr emissions, and is a requirement for assessing the consequence of environmental
21 impacts. We conducted the temporal trend analysis of atmospheric NH₃ and NO₂ on a national scale



22 since 1980 based on emission data (during 1980-2010), satellite observations (for NH₃ since 2008 and
23 for NO₂ since 2005) and atmospheric chemistry transport modeling (during 2008-2015).

24 Based on the emission data, during 1980-2010, both significant continuous increasing trend of NH₃ and
25 NO_x were observed from REAS (Regional Emission inventory in Asia, for NH₃ 0.17 kg N ha⁻¹ y⁻² and
26 for NO_x 0.16 kg N ha⁻¹ y⁻²) and EDGAR (Emissions Database for Global Atmospheric Research, for
27 NH₃ 0.24 kg N ha⁻¹ y⁻² and for NO_x 0.17 kg N ha⁻¹ y⁻²) over China. Based on the satellite data and
28 atmospheric chemistry transport modeling named as the Model for Ozone and Related chemical
29 Tracers, version 4 (MOZART-4), the NO₂ columns over China increased significantly ($p < 0.01$) from
30 2005 to 2011 and then decreased significantly from 2011 to 2015; the satellite-retrieved NH₃ columns
31 from 2008 to 2014 had no big changes but increased in 2015 (large increase from satellite IASI, but
32 slight increase from MOZART-4). The decrease in NO₂ columns since 2011 may result from more
33 stringent strategies taken to control NO_x emissions during the 12th Five-Year-Plan, while no control
34 policy focused on NH₃ emissions. Our findings provided an overall insight on the temporal trends of
35 both NO₂ and NH₃ since 1980 based on emission data, satellite observations and atmospheric transport
36 modeling. These findings can provide a scientific background for policy-makers that are attempting to
37 control atmospheric pollution in China. Moreover, the multivariate data used in this study have
38 implications for estimating long-term Nr deposition datasets to assess its impact on soil, forest, water
39 and greenhouse balance.

40 **Keywords:** trends, seasonal cycle, ammonia

41 **1. Introduction**

42 Reactive nitrogen (Nr) emissions have increased significantly in China due to anthropogenic activities
43 such as increased combustion of fossil fuels, over-fertilization and high stocking rates of farm animals



44 (Canfield et al., 2010;Galloway et al., 2008;Liu et al., 2013). Elevated Nr in the environment has led to
45 a series of effects on climate change and ecosystems, e.g. biodiversity loss, stratospheric ozone
46 depletion, air pollution, freshwater eutrophication, the potential alteration of global temperature,
47 drinking water contamination, dead zones in coastal ecosystems and grassland seed bank depletion
48 (Basto et al., 2015;Lan et al., 2015;Shi et al., 2015). Atmospheric reactive N emissions are dominated
49 by nitrogen oxides ($\text{NO}_x = \text{NO} + \text{NO}_2$) and ammonia (NH_3) (Li et al., 2016a;Galloway et al., 2004).
50 Atmospheric NO_2 and NH_3 are the most important precursors for Nr compounds including N_2O_5 , HNO_3 ,
51 HONO and particulate NO_3^- and NH_4^+ in the atmosphere (Xu et al., 2015;Pan et al., 2012). Therefore,
52 an understanding of both the spatial and temporal patterns of NO_2 and NH_3 is essential for evaluating
53 N-enriched environmental effects, and can provide the scientific background for N pollution mitigation.
54 To investigate the spatial and temporal variations of atmospheric NO_2 and NH_3 , ground measurements
55 are acknowledged to be an effective way in monitoring the accurate concentrations of NO_2 and NH_3
56 (Xu et al., 2015;Pan et al., 2012;Meng et al., 2010). Ground measurements of NO_2 concentrations in
57 China, including about 500 stations in 74 cities, have been monitored and reported to the public since
58 January 2013 (Xie et al., 2015). By the end of 2013, this network was extended with hourly NO_2
59 concentrations from more than 850 stations in 161 cities. However, there are fewer NH_3 measurements
60 across China than NO_2 measurements. The China Agricultural University has organized a Nationwide
61 Nitrogen Deposition Monitoring Network (NNDMN) since 2004, consisting of 43 monitoring sites
62 covering urban, rural (cropland) and background (coastal, forest and grassland) areas across China (Xu
63 et al., 2015;Liu et al., 2011). Xu et al. (2015) reported the ground NH_3 concentrations throughout China
64 for the first time, providing great potential to understand the ground NH_3 concentrations on a national
65 scale. Other networks include (1) the Chinese Ecosystem Research Network (CERN) which was



66 established in 1988, including 40 field stations (Fu et al., 2010). However, to our knowledge, there are
67 no detailed reports about ground NH₃ concentrations from CERN on a national scale. (2) Four Chinese
68 cities (Xiamen, Xi-An, Chongqing and Zhuhai) have joined the Acid Deposition Monitoring Network
69 in East Asia (EANET) since 1999. However, only one site (Hongwen, Xiamen) in EANET measured
70 the ground NH₃ concentrations and that data is not continuous. Finally, ground NH₃ concentrations at
71 ten sites in Northern China from 2007 to 2010 have been reported by Pan et al (2013). All of the above
72 ground measurements provide the potential to understand NH₃ and NO₂ concentrations on a regional
73 scale. However, there is limited information on the spatial and temporal variations of NH₃ and NO₂ in
74 the atmosphere across China. This is due to the limited observation sites and monitoring period, as well
75 as given the uneven distribution of the monitoring sites. Importantly, atmospheric NH₃ and NO₂
76 monitoring based on ground-based local sites may have limited spatial representativeness of the
77 regional scale as both NH₃ and NO₂ are highly variable in time and space (Clarisse et al., 2009; Wichink
78 Kruit et al., 2012; Boersma et al., 2007).

79 In order to complement ground-based measurements, satellite observation of NH₃ and NO₂ is a
80 welcome addition for analyzing the recent trends of NH₃ and NO₂ in the atmosphere. Satellite remote
81 sensing offers an opportunity to monitor atmospheric NH₃ and NO₂ with high temporal and spatial
82 resolutions (Warner et al., 2017; Li et al., 2016b). NO₂ was measured by multiple space-based
83 instruments including the Global Ozone Monitoring Experiment (GOME), SCanning Imaging
84 Absorption SpectroMeter for Atmospheric CHartographY (SCIAMACHY), Ozone Monitoring
85 Instrument (OMI) and Global Ozone Monitoring Experiment-2 (GOME-2). The OMI NO₂ provides the
86 best horizontal resolution (13 × 24 km²) among instruments in its class and near-global daily coverage
87 (Levelt et al., 2007). OMI observations have been widely applied in environmental-related studies and



88 for the support of emission control policy (Russell et al., 2012; Zhao and Wang, 2009). First
89 measurements of NH_3 from space were reported over Beijing and San Diego areas with the
90 Tropospheric Emission Spectrometer (TES) (Beer et al., 2008) and in fire plumes in Greece with the
91 Infrared Atmospheric Sounding Interferometer (IASI) (Coheur et al., 2009). The first global map of
92 NH_3 was created from IASI measurements by correlating the observed brightness temperature
93 differences to NH_3 columns using the averaged datasets in 2008 (Clarisse et al., 2009). Shortly after
94 that, many studies focused on developing techniques to gain more reliable NH_3 columns (Whitburn et
95 al., 2016a; Van Damme et al., 2014b), validating the retrieved NH_3 columns using the ground
96 measurements (Van Damme et al., 2014a; Dammers et al., 2016) and comparing the data with the
97 results of the atmospheric chemistry transport models (Van Damme et al., 2014c; Whitburn et al.,
98 2016a), and the estimated NH_3 columns obtained from Fourier transform infrared spectroscopy (FTIR)
99 (Dammers et al., 2016). The current method is based on the calculation of a spectral hyperspectral
100 range index and subsequent conversion to a NH_3 total column using a neural network. Details on the
101 retrieval algorithm can be found in Whitburn et al. (2016). The progresses made on the satellite
102 techniques provides potential for understanding both the spatial and temporal variations of NH_3 and
103 NO_2 in the atmosphere.

104 In addition to satellite observations, the emission data are also very important tools for investigating the
105 temporal trends of NH_3 and NO_2 such as the IIASA inventory (Cofala et al., 2007), EDGAR (Emission
106 Database for Global Atmospheric Research, RAINS-Asia (Regional Air Pollution Information and
107 Simulation) and Asia REAS (Regional Emission inventory in Asia). REAS is considered as the first
108 inventory by integrating historical, current and future emissions data for Asia based on a consistent
109 methodology (Ohara et al., 2007), and EDGAR is the global emission data with 0.1 by 0.1 grid, which



110 is believed to have the highest spatial resolutions among different datasets mentioned above. Thus,
111 REAS and EDGAR are used to analyze the historical trends of NH_3 and NO_2 during 1980-2010 in this
112 study. Based on the EDGAR emission data, a widely used atmospheric transport model named as the
113 Model for Ozone and Related chemical Tracers, version 4 (MOZART-4) was also used to model the
114 temporal trend of NH_3 and NO_2 columns during 2008-2015 in comparison with the temporal trends of
115 NH_3 and NO_2 columns measured by satellite instruments.

116 We aim at getting an overall insight on the temporal trends of both NO_2 and NH_3 since 1980 based on
117 the multivariate data including the emission data, satellite observations and atmospheric transport
118 modeling. We herein show the Chinese national trend of REAS and EDGAR NH_3 and NO_x emission
119 data during 1980-2010, satellite-retrieved NH_3 during 2008-2015 and NO_2 columns (2005-2015), and
120 atmospheric transport chemistry modeling NH_3 and NO_2 columns (2008-2015). It should be noted here
121 that the satellite NH_3 columns were retrieved from the IASI, and can only be obtained since 2008. It is
122 beneficial to analyze the temporal variations of both NH_3 and NO_2 , hence providing a scientific basis
123 for policy makers to reduce N-enriched environmental pollution in China.

124 **2. Materials and methods**

125 **2.1. NH_3 and NO_2 Emissions**

126 We examined the emission inventory dataset for Asia REAS (Regional Emission inventory in Asia)
127 with $0.5^\circ \times 0.5^\circ$ resolution for the period 1980-2010, and analyzed the temporal trends of NO_x and NH_3
128 over China. REAS is believed to be the first inventory of integrating past, present and future dataset in
129 Asia based on a consistent methodology. The REAS datasets have been validated by several emissions,
130 and denotes agreement with the recent growth status in Chinese emissions (Ohara et al., 2007). We also
131 collected NO_x and NH_3 emission data from EDGAR (Emissions Database for Global Atmospheric



132 Research) v4.3.1, developed by the Netherlands Environmental Assessment Agency and European
133 Commission Joint Research Centre (JgJ et al., 2002). The EDGAR emissions are calculated on the basis
134 of a point emissions inventory conducted by the International Energy Agency. EDGAR also has a long
135 time period 1980-2010 with the highest spatial resolution globally ($0.1^{\circ} \times 0.1^{\circ}$)
136 (<http://edgar.jrc.ec.europa.eu/overview.php?v=431>).

137 2.2. Satellite observations

138 IASI is a passive remote-sensing instrument operating in nadir mode and measures the infrared
139 radiation emitted by the Earth's surface and the atmosphere (Clarisse et al., 2009). It covers the entire
140 globe twice a day, crossing the equator at a mean solar local time of 9:30 A.M. and P.M, and has an
141 elliptical footprint of 12 by 12 km up to 20 by 39 km depending on the satellite-viewing angle. In this
142 study we use daytime satellite observations as these are more sensitive to NH_3 and are associated with a
143 large positive thermal contrast and a significant amount of NH_3 (Van Damme et al., 2014b; Whitburn et
144 al., 2016a). The availability of measurements is mainly driven by the cloud coverage as only
145 observations with cloud coverage lower than 25% are processed to be a good compromise between the
146 number of data kept for the analysis and the bias due to the effect of clouds. As the amount of daily
147 data is not always sufficient to obtain meaningful distributions (due to cloud cover or the availability of
148 the temperature profiles from the EUMETSAT operational processing chain) (Van Damme et al.,
149 2014b), it is more appropriate to consider monthly or yearly averages for this trend analysis. We
150 consider IASI observations with a relative error below 100% or an absolute error below 5×10^{15} molec.
151 cm^{-2} for analysis over China. For the error, the filtering depends on the use of the data. For example, in
152 this study, when averaging over large areas, we consider IASI observations with a relative error below
153 100% or an absolute error below 5×10^{15} molec. cm^{-2} for analysis over China. Doing this, low columns



154 typical for background conditions with a large relative error but a small absolute error are also taken
155 into account. For other applications, such as comparing with ground measurements, we would
156 recommend to use a threshold of 75% or even 100% relative error. We gained the data upon request
157 from the Atmospheric Spectroscopy Group at Université Libre De Bruxelles
158 (<http://www.ulb.ac.be/cpm/atmosphere.html>). This data can be gridded on 0.1° latitude \times 0.1° longitude
159 (Dammers et al., 2016), 0.25° latitude \times 0.25° longitude (Whitburn et al., 2016a) and 0.5° latitude \times 0.5°
160 longitude (Whitburn et al., 2016b) or even coarser resolutions depending on the usage of the data. For
161 IASI NH₃, we firstly divided China into 0.5° latitude \times 0.5° longitude grid. For each grid cell, we
162 calculated the monthly arithmetic mean by averaging the daily values with observations points within
163 the grid cell. Similarly, we calculated the annual arithmetic mean by averaging the daily values with
164 observations points within the grid cell over the whole year.

165 The NO₂ columns are obtained from the OMI instrument on NASA's EOS Aura satellite globally
166 everyday. We used the generated products by the project "Derivation of Ozone Monitoring Instrument
167 tropospheric NO₂ in near-real time" (DOMINO) to analyze the temporal trends of NO₂ columns over
168 China. In DOMINO products, only the observations with an absolute error below 10^{15} molec. cm⁻² and
169 a cloud radiance fraction below 0.5 were processed for analysis. The retrieval algorithm is described in
170 detail in the manuscript (Boersma et al., 2007) and recent updates can be found in the DOMINO
171 Product Specification Document (http://www.temis.nl/docs/OMI_NO2_HE5_1.0.2.pdf). We used
172 tropospheric NO₂ retrievals from the DOMINO algorithm v2.0. The retrieval quality of NO₂ products
173 are strongly dependent on different aspects of air mass factors, such as radiative transfer calculations,
174 terrain heights and surface albedo. The OMI v2.0 data were mainly improved by more realistic
175 atmospheric profile parameters, and include more surface albedo and surface pressure reference points



176 than before (Boersma et al., 2011;Boersma et al., 2016). The DOMINO NO₂ datasets are available from
177 <http://www.temis.nl/airpollution/no2.html>. We should state in particular that we used directly the
178 DOMINO v2.0 products of monthly means from 2005 to 2015 over China for the trend analysis. The
179 DOMINO NO₂ columns were gridded at a resolution of 0.125 °latitude×0.125 °longitude grid globally,
180 which has been widely used for scientific applications (Ma et al., 2013;Ialongo et al., 2016;Castellanos
181 et al., 2015).

182 To illustrate measurement availability, we presented here some measurement statistics. A total number
183 of cloud-free daytime observations as characterized by the operational IASI processor by year were
184 retrieved in China during 2008-2015 for NH₃ (Fig. 1b). We retrieved more observation numbers after
185 2010 than those during 2008-2009. In 2010, the update of the improved air temperature profiles, cloud
186 properties products and cloud detection, which are important for calculating the thermal contrast,
187 increased the quality of retrieval (Van Damme et al., 2014b;Van Damme et al., 2014c). In November
188 2014, there was another update of the air temperature profiles, cloud properties products and cloud
189 detection for calculating the thermal contrast. For the updates of the IASI-NH₃ data, you can refer to
190 Van Damme et al. (2014b), Van Damme et al. (2014c) and Whitburn et al. (2016). The monthly
191 observation numbers are also presented in Fig. 1a, showing that spring (Mar, Apr and May), summer
192 (Jun, Jul and Aug), autumn (Sep, Oct and Nov) and winter (Dec, Jan and Feb) months represent 29% ,
193 26%, 23% and 21%, respectively. Compared with large variations of observation numbers for NH₃, the
194 observation numbers for NO₂ varied less by year; winter season had the least, while other seasons
195 varied little.

196 **2.3. Atmospheric transport chemistry model**

197 Atmospheric transport chemistry model is also of central importance in modeling the tropospheric NO₂



198 and NH_3 . We applied a widely used atmospheric global atmospheric transport chemistry model named
199 as the Model for Ozone and Related chemical Tracers, version 4 (MOZART-4) to simulate the
200 tropospheric NO_2 and NH_3 columns during 2008-2015 in accordance with the time period of IASI NH_3
201 measurements.

202 The MOZART-4 model is driven by the meteorological data from the NASA Goddard Earth Observing
203 System Model, Version 5 (GEOS-5). The emission data applied for driving the simulations are based on
204 the updated EDGAR emission inventories. 12 bulk aerosol compounds, 39 photolysis, 85 gas species as
205 well as 157 gas-phase reactions were integrated in MOZART-4. The chemical mechanism on N
206 compounds including the NO_2 , NH_3 and aerosols are detailedly integrated to MOZART-4, which is
207 considered to be suitable for tropospheric chemical compositions (Emmons et al., 2010; Pfister et al.,
208 2008; Sahu et al., 2013). The output data used in the current work are temporally varying six hours
209 every day, which were upon request by Louisa Emmons at National Center for Atmospheric Research
210 (NCAR). The monthly means of NO_2 and NH_3 columns were averaged by the daily data, and then used
211 for the trend analysis over China. For more details about MOZART-4, the reader should refer to
212 previous studies (Emmons et al., 2010; Brasseur et al., 1998; Beig and Singh, 2007).

213 **3. Results and discussions**

214 **3.1. NH_3 and NO_2 emissions during 1980-2010**

215 We conducted the temporal analysis of NH_3 and NO_x emissions since 1980 based on REAS and
216 EDGAR. Both significant continuous increasing trend of NH_3 and NO_x were observed from REAS (for
217 NH_3 $0.17 \text{ kg N ha}^{-1} \text{ y}^{-2}$ and for NO_x $0.16 \text{ kg N ha}^{-1} \text{ y}^{-2}$) and EDGAR (for NH_3 $0.24 \text{ kg N ha}^{-1} \text{ y}^{-2}$ and for
218 NO_x $0.17 \text{ kg N ha}^{-1} \text{ y}^{-2}$) over China (Fig. 2). We found relatively consistent increase of NO_x emission
219 from EDGAR and REAS over China, i.e. $0.17 \text{ kg N ha}^{-1} \text{ y}^{-2}$ vs $0.16 \text{ kg N ha}^{-1} \text{ y}^{-2}$, but inconsistency in



220 the magnitude in NH_3 emissions from EDGAR and REAS over China, i.e. $0.24 \text{ kg N ha}^{-1} \text{ y}^{-2}$ vs 0.17 kg
221 $\text{N ha}^{-1} \text{ y}^{-2}$. The increase rate in NH_3 emissions over China from EDGAR was much higher than that
222 from REAS, indicating the magnitude of increase trend in NH_3 over China remains a debate, although
223 their trend values both positive (at this point they are consistent). It implies that, at least, we can
224 conclude that the NH_3 emissions are indeed increasing during 1980-2010. We also conducted a simple
225 correlation analysis of the NH_3 (Fig. 2a) and NO_x (Fig. 2b) from REAS and EDGAR, showing
226 agreement in the magnitude (slope=1.06) and temporal trend ($R^2=0.96$) for NO_x , but some
227 inconsistency in the increase rate (slope=1.33) for NH_3 .
228 Aforementioned explanations suggest the NH_3 emissions in China since 1980 remains a debate in the
229 magnitude of NH_3 increase rate from REAS and EDGAR. Liu et al. (2013) conducted that emissions of
230 national anthropogenic NH_3 and NO_x summarized from published data during 1980-2010, and found
231 that the NH_3 emissions increase rate was about 0.32 Tg N y^{-2} (about $0.33 \text{ kg N ha}^{-1} \text{ y}^{-2}$), which was
232 close to $0.24 \text{ kg N ha}^{-1} \text{ y}^{-2}$ from EDGAR. At this point, it seems that the trend in NH_3 emissions from
233 EDGAR over China since 1980 may be more reasonable, but should be further to be validated in the
234 future due to the fact that it may be not appropriate to compare the gridded emission map from EDGAR
235 or REAS with the results of statistical data conducted from published papers by Liu et al. (2013).

236 3.2. Satellite NH_3 and NO_2 over China in the recent decade

237 3.2.1. Temporal trends

238 We used the average values over the whole China by month to demonstrate the trend analysis. From
239 satellite observations, the NO_2 columns over China increased significantly with a slope of $0.011 (10^{15}$
240 $\text{ molec. cm}^{-2} \text{ month}^{-1})$ from January 2005 to December 2011 and then decreased significantly with a
241 slope of $-0.017 (10^{15} \text{ molec. cm}^{-2} \text{ month}^{-1})$ from January 2011 to December 2015 (Fig. 3 a). The



242 decreasing trends were consistent with NO_x emissions since 2011 over China (decreasing from
243 24.04×10⁶ ton in 2011 to 20.78 ×10⁶ ton in 2014, China Statistical Yearbook, <http://www.stats.gov.cn/>).
244 The decrease percentage in NO_x emissions was 16.67% from 2011 to 2014, which was consistent with
245 the decrease percentage (17.86%) in the NO₂ columns from 2011 to 2014 over China. During the
246 Chinese 11th Five-Year-Plan (11th FYP) period (2006-2010), even though Chinese government
247 undertook a series of strategies to increase energy efficiency and to reduce NO_x emissions, NO_x
248 emissions were not restrained, creating a big challenge for improving air quality over the country (Xia
249 et al., 2016). During the 12th FYP period (2011-2015), more stringent strategies were taken to control
250 NO_x emissions, including the application of selective catalytic/non-catalytic reduction (SCR/SNCR)
251 systems in the power sector, staged implementation of tighter emission standards on vehicles and a
252 series of standards with aggressive emission limits for power, cement, and the iron and steel industries.
253 These strategies are believed to have helped achieve national targets of NO_x emission abatement (Xia et
254 al., 2016).
255 However, the satellite-retrieved NH₃ columns had no big changes (increased slightly with a slope of
256 0.024 × 10¹⁵ molec. cm⁻² month⁻¹ from 2008 to 2014 (Fig. 3 b), but increase largely in 2015 (this will
257 be discussed in Sect. 3.3 in comparison with MOZART-4 simulations in detail). No decreasing trend in
258 NH₃ columns may be associated with continuous N fertilizer use for guaranteeing increase of crop
259 productions (Erisman et al., 2008). Although there was no strong NH₃ emission control regulation, N
260 fertilizer efficiency should be further improved over China. In 2015, the Ministry of Agriculture
261 formally announced a “Zero Increase Action Plan” for national fertilizer use by 2020, which requires
262 the annual increase in total fertilizer use will be less than 1% from 2015 to 2019, with no further
263 increment from 2020 (Liu et al., 2015).



264 If the “Zero Increase Action Plan” for N fertilizer can be effective, future NH₃ emissions should be
265 consistent with the current NH₃ emissions. In addition, due to strong emission control of NO_x, the NO_x
266 emissions were believed to decrease significantly from 2011 to 2015. We can reasonably make two
267 major conclusions. First, the atmospheric NO₂, as a key indicator of oxidized N compounds (NO₂,
268 HNO₃ and NO₃⁻), decreased since 2011, which was consistent with the results of Xia et al. (2016), and
269 will continue to decrease under the current policy. Second, the atmospheric NH₃, as a key indicator of
270 reduced N (NH₃ and particulate NH₄⁺), will slightly increase or stay at the current level in the future
271 with the “Zero Increase Action Plan”. Thus, due to a decreasing trend of oxidized N (NO_x-N), ammonia
272 N (NH_x-N) should still dominate Nr deposition (oxidized N plus ammonia N) in China, and is expected
273 to play a more significant role in Nr deposition. Therefore, monitoring the reduced N on a regional
274 scale is encouraged to assist in enacting effective measures to protect the environments and public
275 health, with respect to air, soil and water quality.

276 3.2.2. Spatial pattern

277 High NH₃ columns were found in Beijing, Hebei, Henan, Shandong, Hubei and Jiangsu provinces and
278 in Eastern Sichuan province (Fig. 4a), which were consistent with their high NH₃ emissions due to
279 intensive fertilizer application and livestock (Huang et al., 2012). Guangdong, Guangxi, Hunan and
280 Jiangxi provinces also showed high NH₃ columns, due to high volatilization from paddy fields in these
281 regions, with rice being the dominant crop and contributing the most emissions. The high NH₃ columns
282 are in agreement with the high percent farmland area (Fig. S1), reflecting China’s unique agricultural
283 structure and farming practice. In details, the high NH₃ columns in southern China are in agreement
284 with the high percent paddy farmland area (Fig. S1a) and the high NH₃ columns in northern China are
285 in agreement with the high percent dry farmland area (Fig. S1b). In addition, the NH₃ emissions from



286 vehicles in urban areas could also contribute to the observed high NH_3 columns. For example, in
287 Beijing, the contribution of vehicles equipped with catalytic converters, particularly since the
288 introduction of three-way-catalysts, to non-agricultural NH_3 emissions has recently been considered
289 and might be the most important factor influencing NH_3 concentrations in urban cities (Meng et al.,
290 2011). In addition, middle-level NH_3 columns were also observed in some regions in Xinjiang province,
291 although small percent farmland existed there. This is mainly due to the fact that the NH_3 emissions
292 from livestock exceeded those from the farmland in Xinjiang, and the contribution of livestock to the
293 total NH_3 emissions in Xinjiang accounted for higher than 66% (Huang et al., 2012;Zhou et al., 2015).
294 Xinjiang province, where sheep are widely raised, also emits remarkable NH_3 emissions related to
295 sheep manure management (Huang et al., 2012;Kang et al., 2016). The lower NH_3 columns are located
296 mostly in the Tibet Plateau area, where there is a minimal amount of arable land and low use of
297 synthetic nitrogenous fertilizers.

298 NO_2 columns (Fig. 4b) show significantly higher values over vast areas covering North China, East
299 China, and the Sichuan Basin. The NO_2 columns also show high values over the Pearl River Delta, the
300 southern part of Northeast China, and some areas in Northwest China. High NO_2 columns are mostly
301 distributed in populated areas (Fig. S2), where there is a mix of various anthropogenic NO_x sources,
302 such as vehicles and industrial complexes (Wang et al., 2012;Xu et al., 2015;Meng et al., 2010). It
303 should be noted that an enhanced emission intensity from transportation is confirmed since 2005, even
304 with staged implementation of tightened emission standards for on-road vehicles (Wang et al., 2012).
305 For example, NO_x emissions from transportation grew to 30% for the whole country in 2014, and the
306 values reached 44%, 55%, and 33% for Beijing, Shanghai, and Guangdong, respectively. Therefore,
307 transportation is believed to play an increasingly important role in regional NO_2 pollution, especially



308 when emissions from stationary sources are gradually controlled through increased penetration of
309 selective catalytic/non-catalytic reduction (SCR/SNCR) systems.

310 **3.2.3. Limitations of satellite observations**

311 It is better to show the trends of NO_2 and NH_3 by daily data, but satellite instruments are strongly
312 dependent on the meteorological conditions such as cloud fractions or the availability of the
313 temperature profiles (Van Damme et al., 2014b; Boersma et al., 2011), and we cannot retrieve the whole
314 coverage based on daily data over China. It will be beneficial to analyze a very local region with
315 enough numbers of observations, but not appropriate to analyze such large coverage over China. Facing
316 this big challenge, we used the monthly data for the trend analysis over China. The uncertainty of
317 DOMINO v2.0 NO_2 columns has been well documented in Boersma et al. (2011), and the relative error
318 is reported lower than 20-30% in East Asian by an improved altitude-dependent air mass factor look-up
319 table, a more realistic atmospheric profile, an increased number of reference vertical layers and
320 advanced surface albedos (Boersma et al., 2011). The reader is strongly suggested to refer to Boersma
321 et al. (2011) for more details on the uncertainty analysis.

322 The potential uncertainty of IASI NH_3 columns resulted from IASI observation instruments and
323 retrieval algorithms. In this paper, the NH_3 datasets were generated based on the recent-updated robust
324 and flexible NH_3 retrieval algorithms, designed to overcome some shortcomings of the current
325 algorithms (Whitburn et al., 2016a). The current algorithms were designed firstly to calculate the
326 hyperspectral range index (HRI), a measure for the NH_3 signature strength in the spectrum, and then
327 converted to IASI NH_3 columns by using the thermal contrast (TC) and lookup tables (LUT) of (HRI,
328 TC) pair corresponding to NH_3 columns. The retrieval of HRIs is strongly dependent on the amount of
329 NH_3 and the thermal state of the atmosphere (Whitburn et al., 2016a). The quality of the IASI NH_3



330 product has been validated by atmospheric chemistry transport models, ground-based and airborne
331 measurements, and NH_3 total columns obtained with ground-based Fourier transform infrared
332 spectroscopy (FTIR). A first validation of the IASI NH_3 using the LOTOS-EUROS model was
333 conducted over Europe, indicating the respective consistency of IASI measurements and model
334 simulations (Van Damme et al., 2014c). A first evaluation of IASI NH_3 dataset using ground-based
335 measurements was made worldwide, presenting consistency with the available ground-based
336 observations and denoting promising results for evaluation by using independent airborne data (Van
337 Damme et al., 2014a). A first validation of of IASI NH_3 dataset using ground-based FTIR derived NH_3
338 total columns was evaluated, demonstrating a mean relative difference of $-32.4 \pm (56.3)\%$, a correlation
339 r of 0.8 with a slope of 0.73 (Dammers et al., 2016).

340 **3.3. Atmospheric chemistry transport model NO_2 and NH_3 columns since 2008**

341 We retrieved the monthly variations of NO_2 and NH_3 columns since 2008 from MOZART, and found (1)
342 consistent increase trend with satellite observations during 2008-2011 and decrease trend during
343 2011-2015 for NO_2 columns (Fig. 5 and 3); (2) no big change in NH_3 columns during 2008-2014 both
344 from MOZART and IASI (Fig. 5 and 3); (3) large increase in NH_3 columns in 2015 from IASI but no
345 big change from MOZART (Fig. 6, 5 and 3) . For point (1) and (2), we have discussed their reasons in
346 Sect. 3.2, and here only focused on interpretation of the difference in NH_3 columns in 2015 from
347 MOZART and IASI.

348 Based on MOZART-4 (the emission data used for modeling is EDGAR, which is very close to the trend
349 conducted by Liu et al, 2013), the NH_3 columns over China were slightly higher in 2015 than in 2014
350 (6.66×10^{15} molec. cm^{-2} year $^{-1}$ in 2014 vs 6.92×10^{15} molec. cm^{-2} year $^{-1}$ in 2015) as shown in Fig. 5 (b)
351 and (d) referring to the whole coverage in Fig. 4 (a). But the IASI NH_3 columns increased sharply from



352 2014 to 2015 over China (6.59×10^{15} molec. cm^{-2} year^{-1} in 2014 vs 9.08×10^{15} molec. cm^{-2} year^{-1} in
353 2015), as shown in Fig. 5 (a) and (c). At the current state, we can, at least, draw a conclusion that the
354 NH_3 columns over China indeed increased in 2015 both from IASI and MOZART, but just a debate or
355 consistency exists on the increase rate of the NH_3 columns in 2015. This may be still an open question
356 on this point, here we only show this two possibilities and possible reasons. We should clarify in
357 particular we do not aim at validating which is right or wrong from IASI and MOZART (which may be
358 beyond the discussion in this paper), but the NH_3 columns in 2015 indeed increased both from IASI
359 and MOZART and this is the conclusion we really concerned. We should state in particular again that
360 the following discussion in this paragraph was all hypothetical and should be tested in the future work.
361 We leave them open questions, which certainly should be studied in detail in the future. For IASI NH_3
362 columns, the sharp increase in 2015 over China may be an artifact, which may be due to an update of
363 the input data. Similar jumps in IASI NH_3 increase in 2015 can also be visible in the USA and
364 European (Fig. 7), indicating that it may be necessary for a recalculation of the earlier input datasets
365 used for calculating the IASI NH_3 columns since November, 2014.

366 **3.4. Implications for estimating long-term Nr deposition datasets**

367 We found both the NO_2 and NH_3 emissions over China increased continuously from 1980 to 2010
368 based on emissions data from REAS and EDGAR. For NH_3 , based on the satellite observations and
369 atmospheric transport model (MOZART-4), we found high-level NH_3 columns with no big variations
370 from 2008 to 2014 (an increase in 2015 both from IASI and MOZART but large increase from IASI
371 and slight increase from MOZART). For NO_2 , we found continuous high-level NO_2 columns over
372 China from 2005-2011 but a decrease from 2011 to 2015. Despite the decline, the NO_2 columns during
373 2011-2015 were still in high level. Notably, these emissions certainly lead to the deposition of



374 atmospheric Nr in form of dry and wet processes into aquatic ecosystems and terrestrial, with
375 implications affecting ecosystem and human health, biological diversity and greenhouse gas balances
376 (Lu et al., 2016). Hence, it is very crucial to estimate Nr deposition with high spatiotemporal
377 resolutions in order to drive ecological models such as the Denitrification-Decomposition (DNDC)
378 model and Integrated Biosphere Simulator (IBIS), to assess its impact on soil, forest, water and
379 greenhouse balance. Despite progress in satellite techniques in recent decades (for NO₂ since 1997 by
380 GOME and for NH₃ since 2008 by IASI), challenge still exists in estimating both the dry (NO₂, HNO₃
381 particulate NO₃⁻) and wet (NH₄⁺ and NO₃⁻ in precipitation) depositions for a long-term dataset such as
382 since 1980 or earlier possibly due to the complex scheme of N transformations and transportation or
383 limited available data both from emissions, satellites and a limited number of ground measurements.
384 Hence, we call for a long-term dataset of Nr depositions both regionally and globally to investigate
385 how the N emissions affect the environment. Possibly, long-term emissions data such as REAS and
386 EDGAR will provide a valuable dataset to expand the modeling Nr depositions in recent years, while
387 the simulations combining the satellite measurements and CTM model output to derive Nr depositions
388 (Geddes and Martin, 2017; Nowlan et al., 2014) in recent years will provide relatively accurate datasets
389 (certainly need to be validated and modified by ground measurements).

390 **4. Conclusion**

391 Atmospheric ammonia (NH₃) and nitrogen dioxide (NO₂) play an important role in determining air
392 quality, environmental degradation and climate change. The emission data, satellite observations and
393 atmospheric transport modeling have great potential for understanding the temporal variations of
394 atmospheric NH₃ and NO₂ on a regional scale, with high spatial and temporal resolutions. This study



395 analyzed the characteristics of atmospheric NH_3 and NO_2 over China since 1980 based on the
396 multivariate data. The major findings were as follows:

397 1. Based on emission data, both significant continuous increasing trend of NH_3 and NO_x were observed
398 from REAS (for NH_3 $0.17 \text{ kg N ha}^{-1} \text{ y}^{-2}$ and for NO_x $0.16 \text{ kg N ha}^{-1} \text{ y}^{-2}$) and EDGAR (for NH_3 0.24 kg
399 $\text{N ha}^{-1} \text{ y}^{-2}$ and for NO_x $0.17 \text{ kg N ha}^{-1} \text{ y}^{-2}$) over China during 1980-2010.

400 2. Based on the satellite observations and atmospheric transport model (MOZART-4), we found
401 continuous high-level NH_3 columns with no big variations in NH_3 columns from 2008 to 2014 (an
402 increase in 2015 both from IASI and MOZART but large increase from IASI and slight increase from
403 MOZART). For NO_2 , we found continuous high-level NO_2 columns over China from 2005-2011 but a
404 decrease from 2011 to 2015 (still in high level). The decrease of NO_2 columns may result from more
405 stringent strategies taken to control NO_x emissions during the 12th Five-Year-Plan, including
406 successful application of SCR/SNCR systems in the power sector, tighter emission standards on
407 vehicles and a series of standards with aggressive emission limits. No decreasing trend of NH_3 columns
408 may be due to continuous N fertilizer use for guaranteeing continuous increase of the crop productions.

409 **Acknowledgements**

410 We acknowledge the free use of tropospheric NO_2 column data from the OMI sensor from
411 www.temis.nl. The NH_3 data have been obtained by the Atmospheric Spectroscopy Group at Université
412 Libre de Bruxelles (ULB) (<http://www.ulb.ac.be/cpm/atmosphere.html>). S. Whitburn and M. Van
413 Damme are acknowledged for making the data available and for their help in how to use them. We also
414 thank Louisa Emmons from National Center for Atmospheric Research (NCAR) for providing the
415 MOZART output data for the trend analysis. This study is supported by the National Natural Science
416 Foundation of China (No. 41471343 and 41101315).



417 **Reference**

- 418 Basto, S., Thompson, K., Phoenix, G., Sloan, V., Leake, J., and Rees, M.: Long-term nitrogen
419 deposition depletes grassland seed banks, *Nature Communication*, 6, 1-6, 10.1038/ncomms7185, 2015.
- 420 Beer, R., Shephard, M. W., Kulawik, S. S., Clough, S. A., Eldering, A., Bowman, K. W., Sander, S. P.,
421 Fisher, B. M., Payne, V. H., Luo, M., Osterman, G. B., and Worden, J. R.: First satellite observations of
422 lower tropospheric ammonia and methanol, *Geophysical Research Letters*, 35, n/a-n/a,
423 10.1029/2008GL033642, 2008.
- 424 Beig, G., and Singh, V.: Trends in tropical tropospheric column ozone from satellite data and MOZART
425 model, *Geophysical Research Letters*, 34, 2007.
- 426 Boersma, K., Eskes, H., Veefkind, J. P., Brinksma, E., Van Der A, R., Sneep, M., Van Den Oord, G.,
427 Levelt, P., Stammes, P., and Gleason, J.: Near-real time retrieval of tropospheric NO₂ from OMI,
428 *Atmospheric Chemistry and Physics*, 7, 2103-2118, 2007.
- 429 Boersma, K. F., Eskes, H. J., Dirksen, R. J., van der A, R. J., Veefkind, J. P., Stammes, P., Huijnen, V.,
430 Kleipool, Q. L., Sneep, M., Claas, J., Leitão, J., Richter, A., Zhou, Y., and Brunner, D.: An improved
431 tropospheric NO₂ column retrieval algorithm for the Ozone Monitoring Instrument, *Atmospheric*
432 *Measurement Techniques*, 4, 1905-1928, 10.5194/amt-4-1905-2011, 2011.
- 433 Boersma, K. F., Vinken, G. C. M., and Eskes, H. J.: Representativeness errors in comparing chemistry
434 transport and chemistry climate models with satellite UV-Vis tropospheric column retrievals, *Geosci.*
435 *Model Dev.*, 9, 875-898, 10.5194/gmd-9-875-2016, 2016.
- 436 Brasseur, G., Hauglustaine, D., Walters, S., Rasch, P., Müller, J. F., Granier, C., and Tie, X.: MOZART,
437 a global chemical transport model for ozone and related chemical tracers: 1. Model description, *Journal*
438 *of Geophysical Research: Atmospheres* (1984–2012), 103, 28265-28289, 1998.
- 439 Canfield, D. E., Glazer, A. N., and Falkowski, P. G.: The Evolution and Future of Earth's Nitrogen
440 Cycle, *Science*, 330, 192-196, 10.1126/science.1186120, 2010.
- 441 Castellanos, P., Boersma, K. F., Torres, O., and De Haan, J. F.: OMI tropospheric NO₂ air mass factors
442 over South America: effects of biomass burning aerosols, *Atmospheric Measurement Techniques*, 8,
443 2683-2733, 2015.
- 444 Clarisse, L., Clerbaux, C., Dentener, F., Hurtmans, D., and Coheur, P.-F.: Global ammonia distribution
445 derived from infrared satellite observations, *Nature Geoscience*, 2, 479-483, 2009.



446 Cofala, J., Amann, M., Klimont, Z., Kupiainen, K., and Höglund-Isaksson, L.: Scenarios of global
447 anthropogenic emissions of air pollutants and methane until 2030, *Atmospheric Environment*, 41,
448 8486-8499, <http://dx.doi.org/10.1016/j.atmosenv.2007.07.010>, 2007.

449 Coheur, P.-F., Clarisse, L., Turquety, S., Hurtmans, D., and Clerbaux, C.: IASI measurements of
450 reactive trace species in biomass burning plumes, *Atmospheric Chemistry and Physics*, 9, 5655-5667,
451 2009.

452 Damers, E., Palm, M., Van Damme, M., Vigouroux, C., Smale, D., Conway, S., Toon, G. C., Jones,
453 N., Nussbaumer, E., Warneke, T., Petri, C., Clarisse, L., Clerbaux, C., Hermans, C., Lutsch, E., Strong,
454 K., Hannigan, J. W., Nakajima, H., Morino, I., Herrera, B., Stremme, W., Grutter, M., Schaap, M.,
455 Wichink Kruit, R. J., Notholt, J., Coheur, P. F., and Erisman, J. W.: An evaluation of IASI-NH₃ with
456 ground-based Fourier transform infrared spectroscopy measurements, *Atmos. Chem. Phys.*, 16,
457 10351-10368, 10.5194/acp-16-10351-2016, 2016.

458 Emmons, L., Walters, S., Hess, P., Lamarque, J.-F., Pfister, G., Fillmore, D., Granier, C., Guenther, A.,
459 Kinnison, D., and Laepple, T.: Description and evaluation of the Model for Ozone and Related
460 chemical Tracers, version 4 (MOZART-4), *Geoscientific Model Development*, 3, 43-67, 2010.

461 Erisman, J. W., Sutton, M. A., Galloway, J., Klimont, Z., and Winiwarter, W.: How a century of
462 ammonia synthesis changed the world, *Nature Geoscience*, 1, 636-639, 2008.

463 Fu, B., Li, S., Yu, X., Yang, P., Yu, G., Feng, R., and Zhuang, X.: Chinese ecosystem research network:
464 Progress and perspectives, *Ecological Complexity*, 7, 225-233,
465 <http://dx.doi.org/10.1016/j.ecocom.2010.02.007>, 2010.

466 Galloway, J. N., Dentener, F. J., Capone, D. G., Boyer, E. W., Howarth, R. W., Seitzinger, S. P., Asner,
467 G. P., Cleveland, C. C., Green, P. A., Holland, E. A., Karl, D. M., Michaels, A. F., Porter, J. H.,
468 Townsend, A. R., and Vöösmary, C. J.: Nitrogen Cycles: Past, Present, and Future, *Biogeochemistry*,
469 70, 153-226, 10.1007/s10533-004-0370-0, 2004.

470 Galloway, J. N., Townsend, A. R., Erisman, J. W., Bekunda, M., Cai, Z., Freney, J. R., Martinelli, L. A.,
471 Seitzinger, S. P., and Sutton, M. A.: Transformation of the Nitrogen Cycle: Recent Trends, Questions,
472 and Potential Solutions, *Science*, 320, 889-892, 10.1126/science.1136674, 2008.

473 Geddes, J. A., and Martin, R. V.: Global deposition of total reactive nitrogen oxides from 1996 to 2014
474 constrained with satellite observations of NO₂ columns, *Atmos. Chem. Phys. Discuss.*, 2017, 1-44,
475 10.5194/acp-2016-1100, 2017.



- 476 Huang, X., Song, Y., Li, M., Li, J., Huo, Q., Cai, X., Zhu, T., Hu, M., and Zhang, H.: A high resolution
477 ammonia emission inventory in China, *Global Biogeochemical Cycles*, 26, 1-14, 2012.
- 478 Ialongo, I., Herman, J., Krotkov, N., Lamsal, L., Boersma, K. F., Hovila, J., and Tamminen, J.:
479 Comparison of OMI NO₂ observations and their seasonal and weekly cycles with ground-based
480 measurements in Helsinki, 1-13, 2016.
- 481 Jg, O., Jjm, B., Jahw, P., Bakker, J., Ajh, V., and Jpj, B.: Applications of EDGAR Emission Database
482 for Global Atmospheric Research, Rijksinstituut Voor Volksgezondheid En Milieu Rivm, 2002.
- 483 Kang, Y., Liu, M., Song, Y., Huang, X., Yao, H., Cai, X., Zhang, H., Kang, L., Liu, X., Yan, X., He, H.,
484 Zhang, Q., Shao, M., and Zhu, T.: High-resolution ammonia emissions inventories in China from 1980
485 to 2012, *Atmos. Chem. Phys.*, 16, 2043-2058, 10.5194/acp-16-2043-2016, 2016.
- 486 Lan, Z., Jenerette, G. D., Zhan, S., Li, W., Zheng, S., and Bai, Y.: Testing the scaling effects and
487 mechanisms of N-induced biodiversity loss: evidence from a decade-long grassland experiment,
488 *Journal of Ecology*, 103, 750-760, 10.1111/1365-2745.12395, 2015.
- 489 Levelt, P., Stammes, P., Gleason, J., and Bucsela, E.: Near-real time retrieval of tropospheric NO₂ from
490 OMI, *Atmospheric Chemistry and Physics*, 7, 2103-2118, 2007.
- 491 Li, Y., Schichtel, B. A., Walker, J. T., Schwede, D. B., Chen, X., Lehmann, C. M., Puchalski, M. A.,
492 Gay, D. A., and Collett, J. L.: Increasing importance of deposition of reduced nitrogen in the United
493 States, *Proceedings of the National Academy of Sciences*, 113, 5874-5879, 2016a.
- 494 Li, Y., Thompson, T. M., Van Damme, M., Chen, X., Benedict, K. B., Shao, Y., Day, D., Boris, A.,
495 Sullivan, A. P., Ham, J., Whitburn, S., Clarisse, L., Coheur, P. F., and Collett Jr, J. L.: Temporal and
496 Spatial Variability of Ammonia in Urban and Agricultural Regions of Northern Colorado, United States,
497 *Atmos. Chem. Phys. Discuss.*, 2016, 1-50, 10.5194/acp-2016-1008, 2016b.
- 498 Liu, X., Duan, L., Mo, J., Du, E., Shen, J., Lu, X., Zhang, Y., Zhou, X., He, C., and Zhang, F.: Nitrogen
499 deposition and its ecological impact in China: An overview, *Environmental Pollution*, 159, 2251-2264,
500 <http://dx.doi.org/10.1016/j.envpol.2010.08.002>, 2011.
- 501 Liu, X., Zhang, Y., Han, W., Tang, A., Shen, J., Cui, Z., Vitousek, P., Erismann, J. W., Goulding, K., and
502 Christie, P.: Enhanced nitrogen deposition over China, *Nature*, 494, 459-462, 2013.
- 503 Liu, X., Vitousek, P., Chang, Y., Zhang, W., Matson, P., and Zhang, F.: Evidence for a Historic Change
504 Occurring in China, *Environmental Science & Technology*, 50, 505-506, 2015.
- 505 Lu, X., Jiang, H., Liu, J., Zhang, X., Jin, J., Zhu, Q., Zhang, Z., and Peng, C.: Simulated effects of



- 506 nitrogen saturation on the global carbon budget using the IBIS model, *Scientific Reports*, 6, 39173,
507 10.1038/srep39173, 2016.
- 508 Ma, J. Z., Beirle, S., Jin, J. L., Shaiganfar, R., Yan, P., and Wagner, T.: Tropospheric NO₂ vertical
509 column densities over Beijing: results of the first three years of ground-based MAX-DOAS
510 measurements (2008–2011) and satellite validation, *Atmospheric Chemistry & Physics*, 13, 1547-1567,
511 2013.
- 512 Meng, Z.-Y., Xu, X.-B., Wang, T., Zhang, X.-Y., Yu, X.-L., Wang, S.-F., Lin, W.-L., Chen, Y.-Z., Jiang,
513 Y.-A., and An, X.-Q.: Ambient sulfur dioxide, nitrogen dioxide, and ammonia at ten background and
514 rural sites in China during 2007–2008, *Atmospheric Environment*, 44, 2625-2631,
515 <http://dx.doi.org/10.1016/j.atmosenv.2010.04.008>, 2010.
- 516 Meng, Z., Lin, W., Jiang, X., Yan, P., Wang, Y., Zhang, Y., Jia, X., and Yu, X.: Characteristics of
517 atmospheric ammonia over Beijing, China, *Atmospheric Chemistry and Physics*, 11, 6139-6151, 2011.
- 518 Nowlan, C., Martin, R., Philip, S., Lamsal, L., Krotkov, N., Marais, E., Wang, S., and Zhang, Q.:
519 Global dry deposition of nitrogen dioxide and sulfur dioxide inferred from space - based measurements,
520 *Global Biogeochemical Cycles*, 28, 1025-1043, 2014.
- 521 Ohara, T., Akimoto, H., Kurokawa, J., Horii, N., Yamaji, K., Yan, X., and Hayasaka, T.: An Asian
522 emission inventory of anthropogenic emission sources for the period 1980–2020, *Atmos. Chem.*
523 *Phys.*, 7, 4419-4444, 10.5194/acp-7-4419-2007, 2007.
- 524 Pan, Y., Wang, Y., Tang, G., and Wu, D.: Wet and dry deposition of atmospheric nitrogen at ten sites in
525 Northern China, *Atmospheric Chemistry and Physics*, 12, 6515-6535, 2012.
- 526 Pfister, G., Emmons, L., Hess, P., Lamarque, J. F., Orlando, J., Walters, S., Guenther, A., Palmer, P., and
527 Lawrence, P.: Contribution of isoprene to chemical budgets: A model tracer study with the NCAR CTM
528 MOZART - 4, *Journal of Geophysical Research: Atmospheres* (1984 - 2012), 113, 2008.
- 529 Russell, A., Valin, L., and Cohen, R.: Trends in OMI NO₂ observations over the United States: effects
530 of emission control technology and the economic recession, *Atmospheric Chemistry and Physics*, 12,
531 12197-12209, 2012.
- 532 Sahu, L., Sheel, V., Kajino, M., Gunthe, S. S., Thouret, V., Nedelec, P., and Smit, H. G.: Characteristics
533 of tropospheric ozone variability over an urban site in Southeast Asia: A study based on MOZAIK and
534 MOZART vertical profiles, *Journal of Geophysical Research: Atmospheres*, 118, 8729-8747, 2013.
- 535 Shi, Y., Cui, S., Ju, X., Cai, Z., and Zhu, Y.-G.: Impacts of reactive nitrogen on climate change in China,



- 536 Scientific Reports, 5, 8118, 10.1038/srep08118
- 537 <http://www.nature.com/articles/srep08118#supplementary-information>, 2015.
- 538 Van Damme, M., Clarisse, L., Dammers, E., Liu, X., Nowak, J., Clerbaux, C., Flechard, C.,
539 Galy-Lacaux, C., Xu, W., and Neuman, J.: Towards validation of ammonia (NH₃) measurements from
540 the IASI satellite, Atmospheric Measurement Techniques, 7, 12125-12172, 2014a.
- 541 Van Damme, M., Clarisse, L., Heald, C., Hurtmans, D., Ngadi, Y., Clerbaux, C., Dolman, A., Erisman,
542 J. W., and Coheur, P.-F.: Global distributions, time series and error characterization of atmospheric
543 ammonia (NH₃) from IASI satellite observations, Atmospheric Chemistry and Physics, 14, 2905-2922,
544 2014b.
- 545 Van Damme, M., Wichink Kruit, R., Schaap, M., Clarisse, L., Clerbaux, C., Coheur, P. F., Dammers, E.,
546 Dolman, A., and Erisman, J.: Evaluating 4 years of atmospheric ammonia (NH₃) over Europe using
547 IASI satellite observations and LOTOS - EUROS model results, Journal of Geophysical Research:
548 Atmospheres, 119, 9549-9566, 2014c.
- 549 Wang, S., Zhang, Q., Streets, D., He, K., Martin, R., Lamsal, L., Chen, D., Lei, Y., and Lu, Z.: Growth
550 in NO_x emissions from power plants in China: bottom-up estimates and satellite observations,
551 Atmospheric Chemistry and Physics, 12, 4429-4447, 2012.
- 552 Warner, J. X., Dickerson, R. R., Wei, Z., Strow, L. L., Wang, Y., and Liang, Q.: Increased atmospheric
553 ammonia over the world's major agricultural areas detected from space, Geophysical Research Letters,
554 n/a-n/a, 10.1002/2016GL072305, 2017.
- 555 Whitburn, S., Van Damme, M., Clarisse, L., Bauduin, S., Heald, C. L., Hadji-Lazaro, J., Hurtmans, D.,
556 Zondlo, M. A., Clerbaux, C., and Coheur, P. F.: A flexible and robust neural network IASI-NH₃
557 retrieval algorithm, Journal of Geophysical Research: Atmospheres, 121, 6581-6599,
558 10.1002/2016JD024828, 2016a.
- 559 Whitburn, S., Van Damme, M., Clarisse, L., Turquety, S., Clerbaux, C., and Coheur, P. F.: Doubling of
560 annual ammonia emissions from the peat fires in Indonesia during the 2015 El Niño, Geophysical
561 Research Letters, 43, 11,007-011,014, 10.1002/2016GL070620, 2016b.
- 562 Wichink Kruit, R. J., Schaap, M., Sauter, F. J., van Zanten, M. C., and van Pul, W. A. J.: Modeling the
563 distribution of ammonia across Europe including bi-directional surface-atmosphere exchange,
564 Biogeosciences, 9, 5261-5277, 10.5194/bg-9-5261-2012, 2012.
- 565 Xia, Y., Zhao, Y., and Nielsen, C. P.: Benefits of China's efforts in gaseous pollutant control indicated



566 by the bottom-up emissions and satellite observations 2000–2014, Atmospheric Environment, 136,
567 43-53, <http://dx.doi.org/10.1016/j.atmosenv.2016.04.013>, 2016.

568 Xie, Y., Zhao, B., Zhang, L., and Luo, R.: Spatiotemporal variations of PM_{2.5} and PM₁₀
569 concentrations between 31 Chinese cities and their relationships with SO₂, NO₂, CO and O₃,
570 Particuology, 20, 141-149, <http://dx.doi.org/10.1016/j.partic.2015.01.003>, 2015.

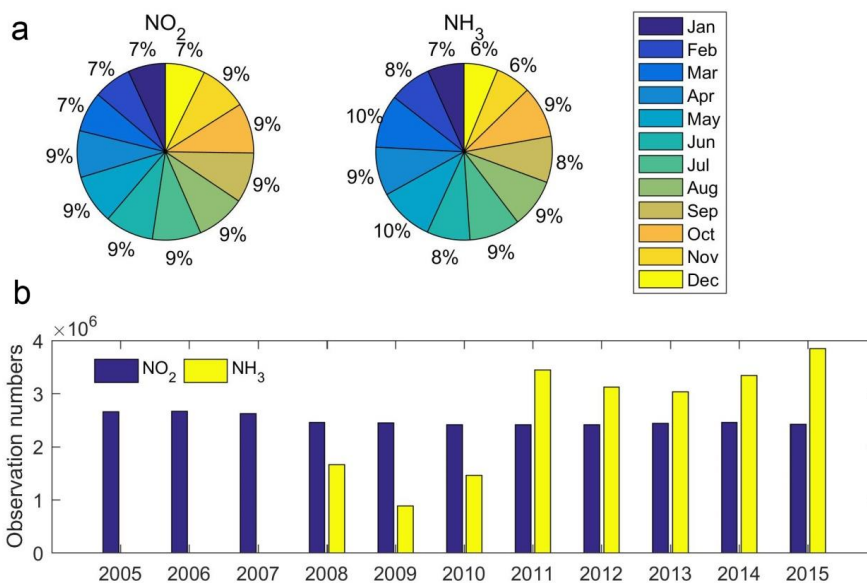
571 Xu, W., Luo, X. S., Pan, Y. P., Zhang, L., Tang, A. H., Shen, J. L., Zhang, Y., Li, K. H., Wu, Q. H., Yang,
572 D. W., Zhang, Y. Y., Xue, J., Li, W. Q., Li, Q. Q., Tang, L., Lv, S. H., Liang, T., Tong, Y. A., Liu, P.,
573 Zhang, Q., Xiong, Z. Q., Shi, X. J., Wu, L. H., Shi, W. Q., Tian, K., Zhong, X. H., Shi, K., Tang, Q. Y.,
574 Zhang, L. J., Huang, J. L., He, C. E., Kuang, F. H., Zhu, B., Liu, H., Jin, X., Xin, Y. J., SHi, X. K., Du,
575 E. Z., Dore, A. J., Tang, S., Collett Jr, J. L., Goulding, K., Sun, Y. X., Ren, J., Zhang, F. S., and Liu, X.
576 J.: Quantifying atmospheric nitrogen deposition through a nationwide monitoring network across China,
577 Atmospheric Chemistry and Physics, 15, 12345-12360, 2015.

578 Zhao, C., and Wang, Y.: Assimilated inversion of NO_x emissions over east Asia using OMI NO₂
579 column measurements, Geophysical Research Letters, 36, 1-5, 2009.

580 Zhou, Y., Shuiyuan, C., Lang, J., Chen, D., Zhao, B., Liu, C., Xu, R., and Li, T.: A comprehensive
581 ammonia emission inventory with high-resolution and its evaluation in the Beijing–Tianjin–Hebei
582 (BTH) region, China, Atmospheric Environment, 106, 305-317,
583 <http://dx.doi.org/10.1016/j.atmosenv.2015.01.069>, 2015.

584

585



586

587

588

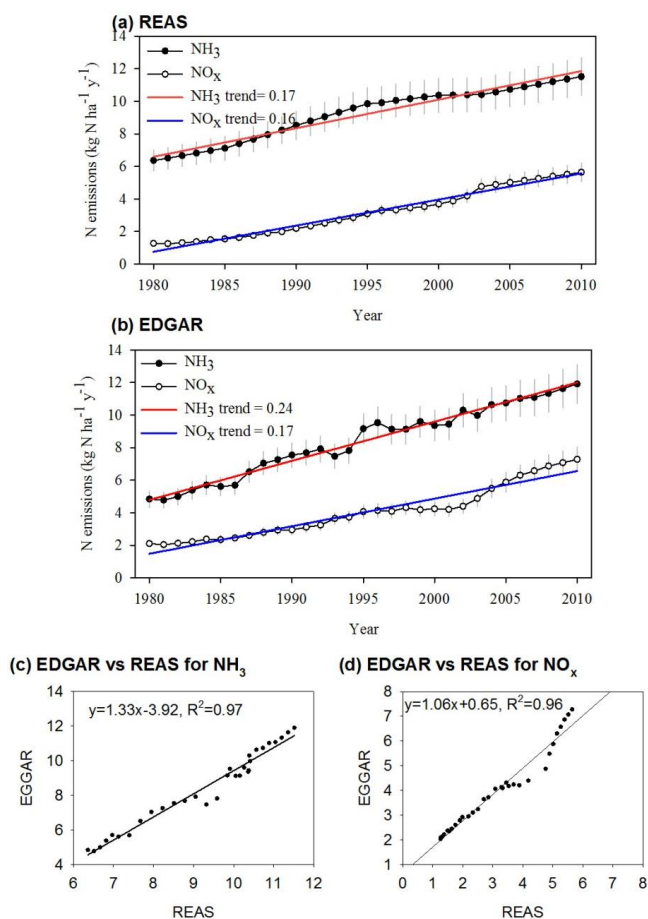
589

590

591

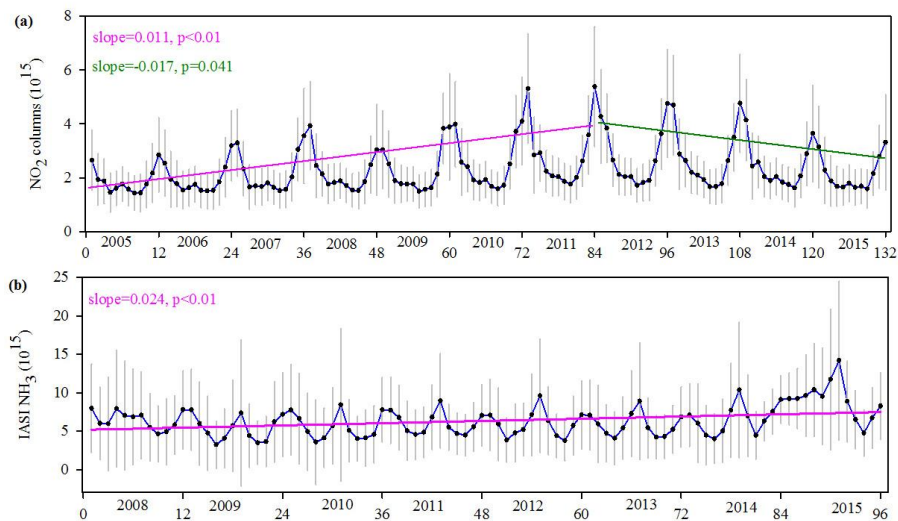
592

Fig. 1. The satellite-derived observation numbers for NO₂ and NH₃. (a) denotes the percentages of observations in each month in 2010 for NO₂ and in 2015 for NH₃ and (b) represents the total observation numbers for NO₂ and NH₃ over China. Notably, the NO₂ observation numbers were gained from DOMINO products, with an absolute error below 10¹⁵ molec. cm⁻² and a cloud radiance fraction below 0.5, while the IASI observations with a relative error below 100% or an absolute error below 5×10¹⁵ molec. cm⁻² were processed for analysis over China.



593

594 **Fig. 2.** The NO_2 and NH_3 emissions over China. (a) denotes the NO_2 and NH_3 emissions over China from 1980 to 2010 from
595 REAS, (b) represents the NO_2 and NH_3 emissions over China from 1980 to 2010 from EDGAR, (c) demonstrates the relationship
596 of NO_2 emissions over China from REAS and EDGAR and (d) shows the relationship of NH_3 emissions over China from REAS
597 and EDGAR.



598

599

600

601

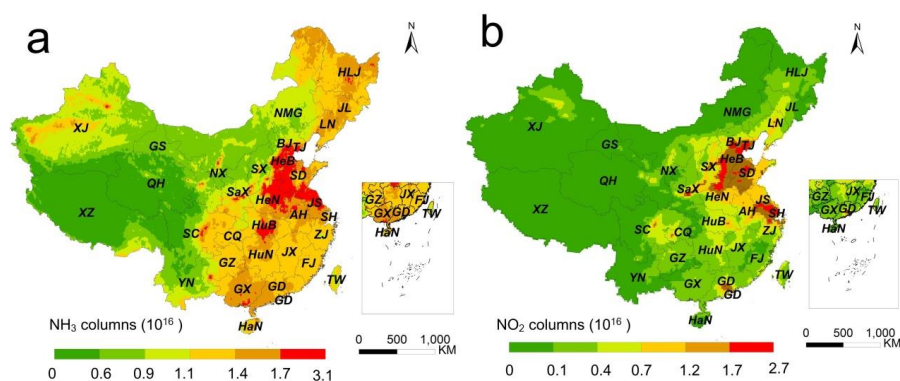
602

603

Fig. 3. Time series of monthly NO_2 columns and NH_3 columns over China. (a) indicates the monthly NO_2 columns from January 2005 to December 2015 and (b) denotes the NH_3 columns from January 2008 to December 2014 over China. The associated mean error for each month is presented here as error bars. Black dots and blue lines indicate the satellite observations, and pink (or green) lines indicate the trend.



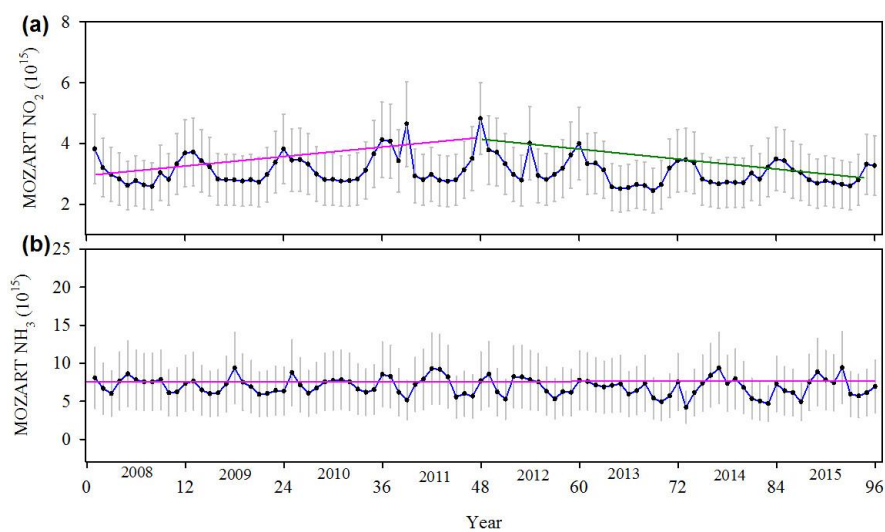
604



605

606 **Fig. 4.** Spatial distribution of the annual NH_3 (a) and NO_2 (b) columns ($\text{molecules cm}^{-2} \text{ year}^{-1}$). The successfully full provincial
607 names are Beijing (BJ), Tianjin (TJ), Hebei (HeB), Shandong (SD), Shanxi (SX), Henan (HeN), Shaanxi (SaX), Liaoning (LN),
608 Jilin (JL), Heilongjiang (HLJ), Neimenggu (NMG), Gansu (GS), Ningxia (NX), Xinjiang (XJ), Shanghai (SH), Jiangsu (JS),
609 Zhejiang (ZJ), Anhui (AH), Hubei (HuB), Hunan (HuN), Jiangxi (JX), Fujian (FJ), Guangdong (GD), Hainan (HaN), Yunnan
610 (YN), Guizhou (GZ), Chongqing (CQ), Sichuan (SC), Guangxi (GX), Xizang (XZ) and Qinghai (QH).

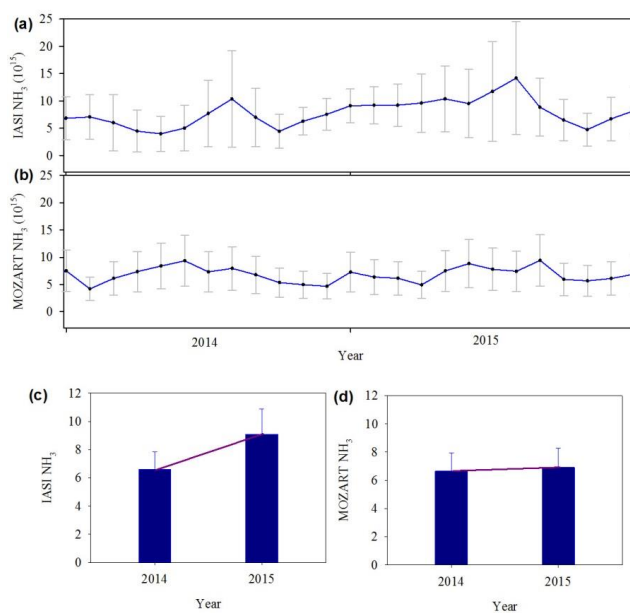
611



612
613 **Fig. 5.** Time series of monthly NO_2 columns (a) and NH_3 columns (b) over China from January 2008 to December 2014 based on
614 MOZART. The associated mean error for each month is presented here as error bars. Black dots and blue lines indicate the
615 satellite observations, and pink (or green) lines indicate the trend.
616

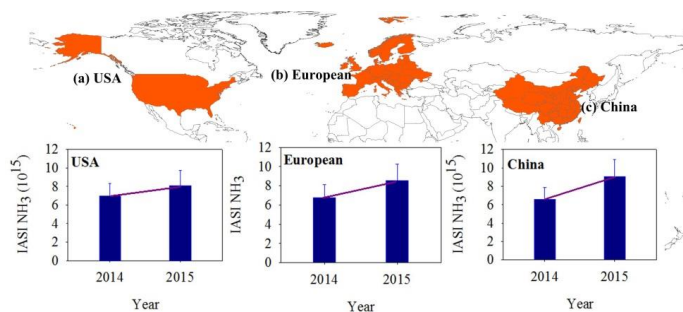


617



618

619 **Fig. 6.** NH₃ columns over China obtained from IASI and MOZART. (a) indicates the variations of monthly NH₃ columns
620 obtained from IASI, (b) denotes the variations of monthly NH₃ columns obtained from MOZART, (c) shows the difference of
621 annual NH₃ columns in 2014 and 2015 obtained from IASI and (d) demonstrates the difference of annual NH₃ columns in 2014
622 and 2015 obtained from MOZART.
623



624

625 **Fig. 7.** IASI NH₃ columns in USA, European and China between 2014 and 2015.

626